Demonstration of Anisotropic Fluid Closure Capturing the Kinetic Structure of Magnetic Reconnection

O. Ohia,[1] J. Egedal,[1,*] V. S. Lukin,[2] W. Daughton,[3] and A. Le[1]

[1]*Plasma Science and Fusion Center, Massachusetts Institute of Technology, Cambridge, Massachusetts 02139, USA*
[2]*Space Science Division, Naval Research Laboratory, Washington, DC 20375, USA*
[3]*Los Alamos National Laboratory, Los Alamos, New Mexico 87545, USA*

(Received 14 April 2012; published 13 September 2012)

Collisionless magnetic reconnection in high-temperature plasmas has been widely studied through fluid-based models. Here, we present results of fluid simulation implementing new equations of state for guide-field reconnection. The new fluid closure accurately accounts for the anisotropic electron pressure that builds in the reconnection region due to electric and magnetic trapping of electrons. In contrast to previous fluid models, our fluid simulation reproduces the detailed reconnection region as observed in fully kinetic simulations. We hereby demonstrate that the new fluid closure self-consistently captures all the physics relevant to the structure of the reconnection region, providing a gateway to a renewed and deeper theoretical understanding of reconnection in weakly collisional regimes.

DOI: 10.1103/PhysRevLett.109.115004 PACS numbers: 52.35.Vd

Magnetic reconnection is a common process in plasmas allowing stress in magnetic fields to be reduced through a rearrangement of the magnetic field line topology. The phenomenon is often accompanied by a large release of magnetic energy which heats the plasma and drives large-scale flows. As such, reconnection is the driver of explosive events, including solar flares, coronal mass ejections, magnetic substorms in Earth's magnetotail, and sawtooth crashes and disruptions in tokamaks [1].

Much theoretical understanding of reconnection has been acquired through the use of fluid models. In particular, two-fluid models, describing the plasma as two separate fluids of electrons and ions [2,3], have been widely used as they reproduce fast reconnection and characteristic ''Hall'' magnetic field structures [4] in weakly collisional regimes, observed by spacecraft in Earth's magnetosphere [5] and in laboratory experiments [6,7]. Also, when comparing two-fluid simulations to results of fully kinetic simulations, good agreement is observed for the rate of reconnection [8]. However, fluid and kinetic codes predict substantially different structure of the reconnection region. For the generic reconnection scenario including a guide magnetic field, kinetic simulations often predict elongated and asymmetric current layers whereas the current layers in two-fluid codes remain mainly symmetric and much shorter. Since these layers can be unstable to secondary reconnection instabilities, these differences have raised doubts about the ability of fluid codes to capture the physics essential to the reconnection process [9].

One of the main difficulties in fluid modeling is to obtain a closure to the hierarchy of fluid equations that is valid in the collisionless limit. A common closure is to assume isothermal electrons with isotropic pressure $p_\parallel = p_\perp = nT_e$. This limit applies to plasmas with infinite heat conduction such that the electron temperature instantaneously equilibrate along magnetic field lines. However, this simple closure is at odds with the anisotropic electron pressure, $p_\parallel \gg p_\perp$, seen in the vicinity of the reconnection region both in kinetic simulations and spacecraft observation [10–13].

Another well-known closure is obtained in the opposite limit where the species are fully magnetized and it is assumed that the plasma has zero heat conduction. In this limit, the double-adiabatic Chew-Goldberger-Low (CGL) scalings result where $p_\parallel \propto n^3/B^2$ and $p_\perp \propto nB$ [14]. The isotropic and CGL models are useful as limiting cases which show the range of anisotropy that can be expected, and they have the advantage that the pressure components are given as explicit functions of n and B. Other, more complicated models have also been considered where the electron pressure is evolved using various closures for the electron heat conductivity. Such models often include separate partial differential equations for evolving the electron pressure components, and, so far, agreement with kinetic simulations has been limited [15,16].

In this Letter, we report on the first self-consistent implementation of a fluid closure applying new equations of state (EOS) for the parallel and perpendicular electron pressures recently derived by Le *et al.* [13]. This closure is obtained in the limit of magnetized electrons with an electron thermal speed much larger than the Alfvén speed, $v_{\mathrm{th},e} \gg v_A$. In this regime the electron motion is adiabatic allowing for an analytical solution $f(v_\parallel, v_\perp)$ to the relevant kinetic equation including the effects of electrons becoming trapped in magnetic wells and by parallel electric fields [17]. Using this analytical solution for $f(v_\parallel, v_\perp)$, Le *et al.* closed the hierarchy of fluid equation and obtained expressions for the parallel and perpendicular pressure in terms of the density, n, and the strength of the magnetic field, B.

The resulting EOS for $p_{\parallel}(n, B)$ and $p_{\perp}(n, B)$ have the following approximate forms:

$$p_{*\parallel} = n_* \frac{2}{2+\alpha} + \frac{\pi n_*^3}{6B_*^2}\frac{2\alpha}{2\alpha+1}, \quad (1)$$

$$p_{*\perp} = n_* \frac{1}{1+\alpha} + n_* B_* \frac{\alpha}{\alpha+1}, \quad (2)$$

where $\alpha = n_*^3/B_*^2$, and for any quantity Q, $Q_* = Q/Q_\infty$, where Q_∞ is the value of Q upstream of the reconnection region.

The analysis by Le *et al.* showed that for $\alpha \ll 1$ the electron behavior is dominated by passing electrons with high heat conduction and the model approach the Boltzmann scaling with $p_{\parallel} = p_{\perp} \propto n_*$. Meanwhile, in the opposite limit, $\alpha \gg 1$, most of the electrons follow trapped trajectories characterized by vanishing heat conduction, and consequently, here the CGL double-adiabatic scalings are approached, $p_{\parallel} \propto n^3/B^2$ and $p_{\perp} \propto nB$. Thus, the new closure represents a smooth transition from Boltzmann scaling at low density and high magnetic field to the CGL scalings at high density and low magnetic field. Le *et al.* showed that the electrons pressures in a kinetic simulations are related to the simulation profiles of n and B as described by the closure; however, the closure was not applied in a self-consistent fluid simulation.

Below we describe the results of the new fluid simulations applying the anisotropic closure for the electron pressure. In addition to this closure we use the regular two-fluid formulation including compressible flows, adiabatic ion pressure, and electron inertia. Hyper-resistivity is included for breaking the frozen-in condition, while ion viscosity and ion thermal conductivity are added for numerical stability. Thus, the full model is described by the following set of equations:

$$\frac{dn}{dt} = -n\nabla\cdot\mathbf{V}_i, \qquad \mu_0\mathbf{J} = \nabla\times\mathbf{B},$$

$$m_i n\frac{d\mathbf{V}_i}{dt} = \mathbf{J}\times\mathbf{B} - \nabla\cdot\bar{\mathbf{P}} + m_i n\nu_i\nabla\cdot\bar{\mathbf{\Theta}},$$

$$\frac{3}{2}\frac{dp_i}{dt} + \frac{5}{2}p_i\nabla\cdot\mathbf{V}_i + m_i n\nu_i\bar{\mathbf{\Theta}}{:}\nabla\mathbf{V}_i = n\kappa_i\nabla^2\left(\frac{p_i}{n}\right),$$

$$\mathbf{B}' = (1-d_e^2\nabla^2)\mathbf{B}, \qquad \frac{\partial\mathbf{B}'}{\partial t} = -\nabla\times\mathbf{E}',$$

$$\mathbf{E}' + \mathbf{V}_i\times\mathbf{B} = \frac{1}{ne}(\mathbf{J}\times\mathbf{B}' - \nabla\cdot\bar{\mathbf{P}}_e) - \eta_H\nabla^2\mathbf{J},$$

$$\bar{\mathbf{P}} = p_i\bar{\mathbf{I}} + \bar{\mathbf{P}}_e = p_i\bar{\mathbf{I}} + p_\perp\bar{\mathbf{I}} + (p_\parallel - p_\perp)\frac{\mathbf{BB}}{B^2},$$

$$\bar{\mathbf{\Theta}} = \nabla\mathbf{V}_i + (\nabla\mathbf{V}_i)^T - \frac{2}{3}(\nabla\cdot\mathbf{V}_i)\bar{\mathbf{I}}.$$

Here, d_e is the electron inertial length, η_H is the hyper-resistivity, and ν_i and κ_i are the ion viscosity and heat conductivity. For simulations with the new fluid closure, $p_{\parallel}$ and $p_{\perp}$ are given by Eqs. (1) and (2), respectively. For isotropic simulations we simply use $p_{\parallel} = p_{\perp} = nT_e$. The equations are implemented numerically using the HiFi multifluid modeling framework [18].

The results of a simulation based on the new closure is presented below and we compare the results to those of a fluid simulation with isotropic pressure and a fully kinetic simulation. For ease of comparison, the three simulations are all applied to the same 2.5 dimensional system (quantities have no gradients in the y direction). The simulations are performed in a doubly-periodic domain of size $L_x \times L_z = 48d_i \times 32d_i$ where $d_i = \sqrt{m_i/\mu_0 n_0 e^2}$ is the ion inertial length. The fluid simulations had 84 grid points per d_i while the kinetic simulation had 192. The initial configuration for the simulations is a double, force-free current sheet with magnetic fields given by

$$B_x(\mathbf{x},0) \simeq B_0\left[\tanh\left(\frac{z+\frac{1}{4}L_z}{\lambda}\right) - \tanh\left(\frac{z-\frac{1}{4}L_z}{\lambda}\right) - 1\right]$$

$$B_y(\mathbf{x},0) = \sqrt{B_0^2 - B_x^2(\mathbf{x},0) + B_{0y}^2}.$$

Lengths are normalized to d_i, while velocities and times are normalized to the Alfvén speed $V_A = B_0/\sqrt{\mu_0 m_i n_0}$ and the ion cyclotron time $\Omega_i = eB_0/m_i$, respectively. The initial current sheet thickness $\lambda = 1$, and the initial upstream guide magnetic field, $B_{0y} = 0.4B_0$. The ion and electron pressures are initially uniform with normalized values $\beta_{i0} = 2p_i\mu_0/B_0^2 = 0.30$ and $\beta_{e0} = 2p_\parallel\mu_0/B_0^2 = 2p_\perp\mu_0/B_0^2 = 0.26$. The mass ratio is $m_i/m_e = 400$. In the fluid simulations, the normalized dissipation parameters are $\eta_H = 1.5\times10^{-5}$, $\nu_i = 3.9\times10^{-2}$ and $\kappa_i = 1.2\times10^{-2}$. The simulation is not sensitive to moderate changes in these parameters; low values hasten the onset of physical and numerical instabilities and high values resemble collisional regimes. Reconnection is seeded with a single X line using an in-plane magnetic field perturbation of amplitude 2.1×10^{-2}.

Before the onset of fast reconnection, the fluid runs yield nearly identical profiles of all quantities independent of the closure used for the electrons, but significant differences develop at later times characterized by fast reconnection. At this later stage, all profiles of the fluid simulation with anisotropic pressure are in excellent agreement with the kinetic simulation results. As an example, Fig. 1 provides two sets of time slices of the out-of-plane current density, J_y, obtained from the three simulation schemes outlined above.

The profiles in Figs. 1(a)–1(c) are obtained at $t\Omega_{ci} = 32$, just after the onset of fast reconnection. At this time, the profiles for the fluid runs are still similar but differences are emerging in the inner reconnection region. Partly due to the intrinsically higher level of numerical noise in kinetic simulations, the onset of reconnection in the kinetic run includes the random formation of a magnetic island that is ejected in the exhaust with $x < 0$. Despite the differences

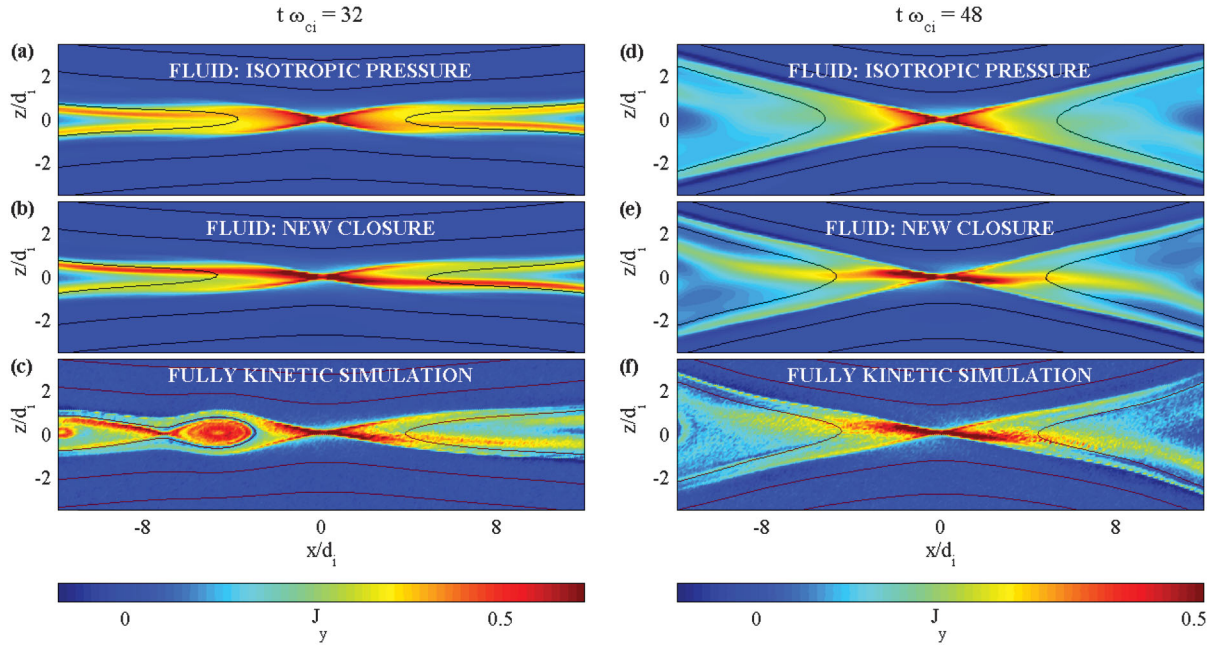

FIG. 1 (color). Out of plane current density profiles for all three simulations at two different simulation times. Solid line represent in-plane magnetic field lines. (a)–(c) Profiles evaluated at $t\Omega_{ci} = 32$. (d)–(f) Profiles evaluated at $t\Omega_{ci} = 48$.

introduced by the island, the profiles of the kinetic run and the anisotropic fluid run are in good agreement for $x > 0$.

For the profiles in Figs. 1(d) and 1(e), evaluated at $t\Omega_{ci} = 48$, the differences in J_y between the fluid simulations are more dramatic. For the isotropic run, the previously observed symmetric structure of the current layer is reproduced, limited in size to a few d_i centered on the X line. In contrast, for the fluid run with the anisotropic pressure, an extended and asymmetric current layer is observed matching the current layer of the fully kinetic simulation (compare Figs. 1(e) and 1(f)).

The agreement between the new fluid model and the kinetic simulation demonstrates that it is the electron pressure anisotropy that is responsible for the elongated electron current layers. The profiles of the pressure anisotropy, $p_\parallel/p_\perp$, for $t\Omega_{ci} = 48$ are shown in Fig. 2 as obtained with the new fluid model and the kinetic simulation. Both simulations yield profiles which are slightly asymmetric towards the diagonal along two of the four separators. Furthermore, the profiles demonstrate good agreement in the magnitude of $p_\parallel/p_\perp$. This agreement has been confirmed in other simulations by varying the initial plasma parameters yielding variable levels of the pressure anisotropy. Suggestive of a scaling law derived for anti-parallel reconnection [19] the pressure anisotropy increases at low values of $\beta_{e\infty}$, where $\beta_{e\infty}$ is the upstream electron pressure normalized to the magnetic field pressure.

To understand the asymmetric structure of $p_\parallel/p_\perp$, it is useful to consider the profiles of B_y, B, and n in Fig. 3 obtained at $t\Omega_{ci} = 48$ from the fluid simulations. Pressure balance in the z direction requires that $\mathbf{B}^2/2\mu_0 + p_\perp + p_i \simeq$ const which regulates the density profile such that n is increased where B is small. Thus, the asymmetries in the profiles of B and n shown in Figs. 3(c)–3(f) are directly related to the asymmetries in how the "Hall" magnetic field adds and subtracts from the

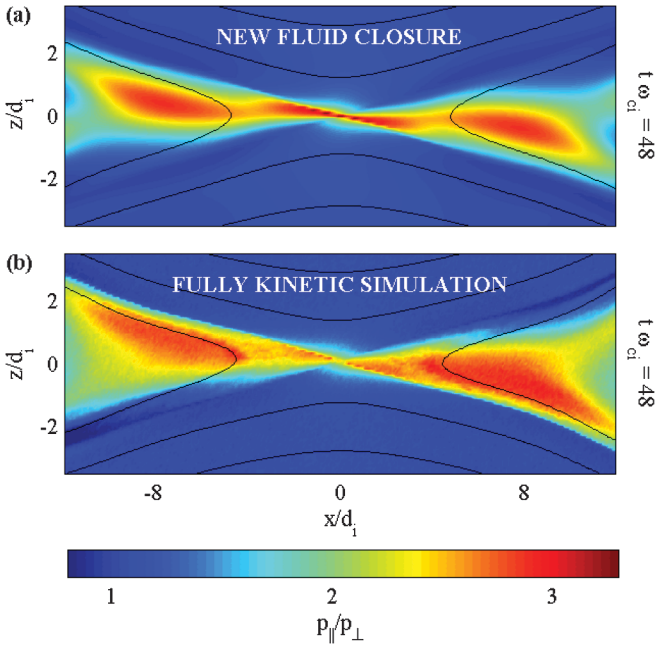

FIG. 2 (color). Ratio of parallel to perpendicular electron pressure $p_\parallel/p_\perp$ for (a) the anisotropic simulation and (b) the particle simulation. Solid lines represent in-plane magnetic field lines.

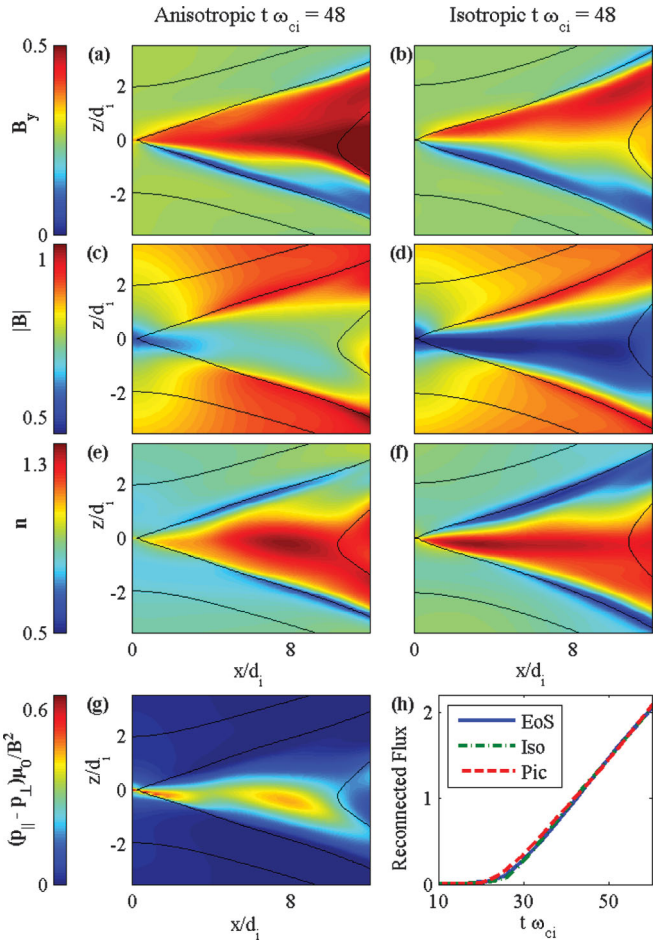

FIG. 3 (color). Comparison between isotropic and anisotropic fluid simulation results of (a),(b) the out of plane magnetic field, (c),(d) the total magnetic field strength, (e),(f) the plasma density and (g) Fire hose stability criterion. For the fire hose stability criterion, a ratio greater than one indicates the region is fire hose unstable. Solid lines represent in-plane magnetic field lines. (h) Time evolution of the reconnected magnetic flux in the fluid simulation with the new equations of state (blue solid line), the isotropic fluid simulation (green dash-dotted line), and the kinetic simulation (red dashed line).

background guide field. In turn, because the profiles of $p_{\parallel}$ and $p_{\perp}$ are related to n and B through the EOS [Eqs. (1) and (2)], this explains the asymmetry observed in $p_{\parallel}/p_{\perp}$.

The pressure anisotropy drives perpendicular currents in the X line region through the additional term $J_{\perp\mathrm{extra}} = [(p_{\parallel} - p_{\perp})/B]\hat{b} \times \hat{b} \cdot \nabla\hat{b}$. Since $\nabla \cdot \mathbf{J} = 0$, it follows that parallel current accounting for the current layer formation is generated by $d(J_{\parallel\mathrm{extra}}/B)/dl = (\nabla \cdot J_{\perp\mathrm{extra}})/B$. Thus, pressure anisotropy influences the magnetic geometry, allowing the magnetic field to simply rotate in the exhaust with only a small reduction in B. Completing a feedback loop, the increased value of B reduces the values of $p_{\parallel} - p_{\perp}$ as predicted by the EOS, allowing the exhaust region to regulate its anisotropy and settle close to the fire hose criterion [Fig. 3(g)] as required for the force balance of a near one-dimensional current sheet [19,20]. In addition, the kinetic simulations can also regulate the anisotropy through pitch angle scattering in cases where fire hose or other instabilities become active in the layer. While the pressure anisotropy is important for the structure of the reconnection region, it does not influence the rate of reconnection [see Fig. 3(h)].

In summary, the new EOS have been implemented in a new fluid simulation and self-consistently reproduce the elongated electron current layer found in kinetic simulations. Furthermore, the fluid and kinetic simulations produce matching electron pressure anisotropy, and reconnection rate, showing that the model captures the essential physics of collisionless, guide-field magnetic reconnection. The fluid model is less computationally expensive compared to the kinetic simulations, but more significantly, the fluid model elucidates the physical processes responsible for setting the structure of the electron current sheets and provides a path forward for properly capturing the microphysics of collisionless magnetic reconnection in macroscopic magnetohydrodynamics-based fluid simulations. Future work will address the applicability of the EOS to three dimensional geometries and the stability of the current layers driven by the pressure anisotropy.

We gratefully acknowledge the computational help and support of Drs. D. Ernst and J. Wright. The work at MIT was funded in part by DOE Grant No. DE-FG02-06ER54878. Contributions from V. S. L. were supported by the Office of Naval Research and the NASA Solar and Heliospheric Physics Program while W. D. was supported by the NASA Heliophysics Theory Program. The simulations were performed using the advanced computing resources at NASA (Pleaides) and NERSC (Hopper).

*jegedal@psfc.mit.edu

[1] E. R. Priest and T. G. Forbes, Astron. Astrophys. Rev. **10**, 313 (2002).
[2] Z. W. Ma and A. Bhattacharjee, Geophys. Res. Lett. **23**, 1673 (1996).
[3] D. Biskamp, E. Schwarz, and J. F. Drake, Phys. Plasmas **4**, 1002 (1997).
[4] B. U. O. Sonnerup, in Magnetic Field *Reconnection in Solar System Plasma Physics*, edited by L. T. Lanzerotti, C. F. Kennel, and E. N. Parker (North-Holland, New York, 1979), Vol. 3, pp. 45–108.
[5] A. L. Borg, M. Oieroset, T. D. Phan, F. S. Mozer, A. Pedersen, C. Mouikis, J. P. McFadden, C. Twitty, A. Balogh, and H. Reme, Geophys. Res. Lett. **32**, 19105 (2005).
[6] Y. Ren, M. Yamada, S. Gerhardt, H. Ji, R. Kulsrud, and A. Kuritsyn, Phys. Rev. Lett. **95**, 055003 (2005).
[7] C. D. Cothran, M. Landreman, M. R. Brown, W. H. Matthaeus, Geophys. Res. Lett. **32**, L03105 (2005).
[8] J. Birn *et al.*, J. Geophys. Res. **106**, 3715 (2001).

[9] W. Daughton, V. Roytershteyn, B. J. Albright, H. Karimabadi, L. Yin, and K. J. Bowers, Phys. Rev. Lett. **103**, 065004 (2009).
[10] M. Oieroset, T. D. Phan, M. Fujimoto, R. P. Lin, and R. P. Lepping, Nature (London) **412**, 414 (2001).
[11] J. Egedal, M. Oieroset, W. Fox, and R. P. Lin, Phys. Rev. Lett. **94**, 025006 (2005).
[12] L. J. Chen *et al.*, J. Geophys. Res. **113**, A12213 (2008).
[13] A. Le, J. Egedal, W. Daughton, W. Fox, and N. Katz, Phys. Rev. Lett. **102**, 085001 (2009).
[14] G. F. Chew *et al.*, Proc. R. Soc. A **236**, 112 (1956).
[15] M. Hesse, M. Kuznetsova, and J. Birn, Phys. Plasmas **11**, 5387 (2004).
[16] J. U. Brackbill, Phys. Plasmas **18**, 032309 (2011).
[17] J. Egedal, W. Fox, N. Katz, M. Porkolab, M. Oieroset, R. P. Lin, W. Daughton, and J. F. Drake, J. Geophys. Res. **113**, A12207 (2008).
[18] V. S. Lukin and M. G. Linton, Nonlinear Proc. Geophys. **18**, 871 (2011).
[19] A. Le, J. Egedal, W. Fox, N. Katz, A. Vrublevskis, W. Daughton, and J. F. Drake, Phys. Plasmas **17**, 055703 (2010).
[20] S. W. H. Cowley, Space Sci. Rev. **26**, 217 (1980).